Acta Histochemica 115 (2013) 649–657

Contents lists available at ScienceDirect

Acta Histochemica

journal homepage: www.elsevier.de/acthis

Morphological changes induced by advanced glycation endproducts in osteoblastic cells: Effects of co-incubation with alendronate

María Virginia Gangoiti[a,*], Pablo Sebastián Anbinder[b], Ana María Cortizo[a], Antonio Desmond McCarthy[a]

[a] LIOMM, Facultad de Ciencias Exactas, Universidad Nacional de La Plata, Calle 47 y 115, CP (1900) La Plata, Argentina
[b] Facultad de Ingeniería, Universidad Nacional de La Plata, Calle 116 y 48, B1900TAG La Plata, Argentina

ARTICLE INFO

Article history:
Received 3 December 2012
Received in revised form 21 January 2013
Accepted 23 January 2013

Keywords:
Osteoblast
Advanced glycation endproducts
Bisphosphonate
Apoptosis
Actin cytoskeleton
Environmental scanning electron microscopy

ABSTRACT

Advanced glycation endproducts (AGEs) accumulate with age in various tissues, and are further increased in patients with *Diabetes mellitus*, in which they are believed to contribute to the development and progression of chronic complications that include a decrease in bone quality. Bisphosphonates are anti-osteoporotic drugs that have been used for the treatment of patients with diabetic bone alterations, although with contradictory results. In the present study, we have evaluated the *in vitro* alterations on osteoblastic morphology by environmental scanning electron microscopy, in actin cytoskeleton and apoptosis induced by AGEs, as well as the modulation of these effects by alendronate (an N-containing bisphosphonate). Our present results provide evidence for disruption induced by AGEs of the osteoblastic actin cytoskeleton (geodesic domes) and significant alterations in cell morphology with a decrease in cell-substratum interactions leading to an increase in apoptosis of osteoblasts and a decrease in osteoblastic proliferation. High concentrations of alendronate (10^{-5} M, such as could be expected in an osteoclastic lacuna) further increase osteoblastic morphological and cytoskeletal alterations. However, low doses of alendronate (10^{-8} M, compatible with extracellular fluid levels to which an osteoblast could be exposed for most of its life cycle) do not affect cell morphology, and in addition are able to prevent AGEs-induced alterations and consequently apoptosis of osteoblasts.

Introduction

Advanced glycation endproducts (AGEs) are implicated in the complications of diabetes and aging (Brownlee, 2005) and are also increased in patients with primary osteoporosis (Hein et al., 2003). Diabetic patients show significantly higher serum AGEs than non-diabetic subjects (Sharp et al., 2003). These products have been involved in the development and progression of diabetic micro- and macroangiopathies (Brownlee, 2005; Barbosa et al., 2008). In addition, AGEs are believed to be partly responsible for the decrease in bone formation and/or turnover observed in patients with type 1 and type 2 *Diabetes mellitus*, which leads to an increased risk of low-stress fractures when compared to the non-diabetic population (Schwartz, 2003).

We have previously shown that soluble and matrix-associated AGEs can inhibit osteoblastic growth and differentiation (McCarthy et al., 1997, 2001). In later studies, we found that accumulation of AGEs on a type I collagen matrix inhibited the integrin-mediated adhesion of UMR-106 osteoblasts (McCarthy et al., 2004), and also induced an increase in cell clumping and a decrease in cellular spreading (unpublished observations).

Bisphosphonates (BP) are anti-osteoporotic drugs whose primary action is to inhibit osteoclast function and survival, although they have also been shown to increase osteoblastic development and thus bone formation (Viereck et al., 2002). Bisphosphonates have been used for the treatment of patients with diabetic bone alterations, although with contradictory results (Dagdelen et al., 2007; Yamauchi, 2007).

In a recent study we showed that low doses (10^{-8} M) of BP completely prevented the AGEs-induced alterations in osteoblast proliferation, differentiation, apoptosis and reactive oxygen species production (Gangoiti et al., 2008). However, high doses of BP (10^{-4}–10^{-5} M) were toxic for osteoblasts.

The actin cytoskeleton plays an important role in determining cell shape, and its reorganization is subject to modulation by interactions with the extracellular matrix (ECM) (Small et al., 1999). The arrangement of actin microfilaments in stress fibers allows the cells to anchor to the substrate by formation of focal adhesions. When an agent interferes with this mechanism, cells show microscopic alterations in their shape, adhere less to the ECM and can subsequently die by apoptosis.

* Corresponding author.
E-mail address: mvgangoiti@biol.unlp.edu.ar (M.V. Gangoiti).

0065-1281/$ – see front matter © 2013 Elsevier GmbH. All rights reserved.
http://dx.doi.org/10.1016/j.acthis.2013.01.004

One important advance in microscopy has been the introduction of the environmental scanning electron microscope (E-SEM) that can operate at very low vacuum and allows the observation of fresh samples without the need for any previous treatment (Stabentheiner et al., 2010). The development of this instrumentation means that whole new classes of materials can now be observed in their natural state (Uroukov and Patton, 2008; Osma et al., 2011).

The focus of the current study was to examine whether the effects of AGEs and alendronate on osteoblastic functionality can be correlated with changes in cell morphology and cytoskeleton. For this study we used UMR-106 osteoblastic cells in culture to evaluate the effect of AGEs and/or alendronate on cellular morphology (observed by E-SEM), on the organization of their actin cytoskeleton (by immunofluorescence) and on the possible modulation of cell proliferation and induction of apoptosis (by comet assay).

Materials and methods

Materials

Alendronate (1-hydroxy-3-aminobutylidene-1,1-bisphosphonic acid) was provided by Elea Laboratories (Buenos Aires, Argentina). Dulbecco's modified Eagle's medium (DMEM), trypsin-EDTA and fetal bovine serum were obtained from Gibco (Invitrogen, Buenos Aires, Argentina). Tissue culture disposable material was supplied by Nunc (Tecnolab, Buenos Aires, Argentina). Centricon 10 kDa cutoff filter cartridges were purchased from Amicon (Beverly, MA, USA). Bovine serum albumin, D-glycolaldehyde and Triton X-100 were obtained from Sigma–Aldrich (Buenos Aires, Argentina). Rat tail acid-soluble type I collagen was purchased from Sigma–Aldrich (St. Louis, MO, USA). Propidium iodide (PI) and FITC-phalloidine were from Molecular Probes (Buenos Aires, Argentina). All other chemicals and reagents were purchased from commercial sources and were of analytical grade.

Preparation of advanced glycation endproducts

AGEs-modified bovine serum albumin was prepared by incubation of 10 mg/ml bovine serum albumin (BSA) with 33 mM D-glycolaldehyde in 150 mM phosphate-buffered saline pH 7.4 at 37 °C for 3 days under sterile conditions, as previously described (Gangoiti et al., 2008). D-Glycolaldehyde was used as the glycating sugar instead of glucose to speed up non-enzymatic glycosylation. Control BSA was incubated in the same conditions without sugar. The non-incorporated sugar was removed by centrifugation/filtration with Centricon filter cartridges. The formation of AGEs was assessed with a LUMEX Fluorat®-02-Panorama spectrofluorometer (St. Petersburg, Russia), using their characteristic fluorescence-emission maximum at 450 nm upon excitation at 370 nm. The estimated level of AGEs-modified BSA obtained in this *in vitro* incubation was 18.5% relative fluorescence intensity/mg protein, in contrast to 3.2% for control BSA.

Preparation of AGE-modified type I collagen for cell matrices and cell proliferation assays

Collagen was solubilized in sterile 0.02 N acetic acid (2.5 mg/ml) (pH 3.0), poured into plastic dishes (50 mg/cm^2) and incubated at 37 °C. Collagen formed a thin film during incubation. The film was washed with phosphate-buffered saline (PBS) and further incubated with or without 100 mM D-glycolaldehyde in PBS at 37 °C for 3 days in sterile conditions (McCarthy et al., 2001). After incubating, collagen contained more AGE-associated fluorescence than control collagen incubated with PBS alone (observed by fluorescence microscopy). Finally, the plates were extensively washed with DMEM to eliminate excess D-glycolaldehyde, and the osteoblastic cells indicated below were plated and incubated in DMEM-10% fetal bovine serum, with or without different doses of alendronate. Cell proliferation was determined using the crystal violet mitogenic bioassay as described previously (Okajima et al., 1992).

Cell cultures and incubations

UMR-106 rat osteosarcoma cells (ATCC, Manassas, VA, USA) were grown in DMEM containing 10% fetal bovine serum, 100 U/ml penicillin and 100 μg/ml streptomycin at 37 °C in a 5% CO_2 atmosphere (McCarthy et al., 1997). Cells were seeded on 75 cm^2 flasks, sub-cultured using trypsin-EDTA and replated on multi-well plates. The UMR106 rat osteosarcoma-derived cell line has been shown to conserve certain characteristics of differentiated osteoblastic phenotype (Partridge et al., 1983). For microscopy evaluations, cells seeded on multi-well plates were incubated in DMEM with different doses of BSA or AGEs-BSA, with or without alendronate, during the periods of time and conditions indicated below.

Environmental scanning electron microscopy (E-SEM)

Information about the attachment and morphology of cells was obtained by E-SEM. When cells growing on multi-well plates reached sub-confluence, the basal medium was removed and replaced by DMEM without serum and with BSA or AGEs (100 μg/ml) in the presence or absence of alendronate (10^{-8} M and 10^{-5} M). Cells were cultured for an additional 24 h, after which they were washed with a PBS solution and then fixed with 5% glutaraldehyde in PBS solution for 10 min. After fixation, the samples were rinsed twice with distilled water to avoid salt precipitation, and observed using a FEI-Quanta 200 Scanning Electron Microscope (Hillsboro, OR, USA) equipped with a gaseous secondary electron detector (GSED) under specific conditions: 12.5 kV, a spot size of 5–6, 5 torr vacuum, 2500× magnification and a 6 mm working distance. To avoid the collapse of cells, a pump-down routine of four cycles of 5/10 torr, finishing at 5 torr, was carried out for a specimen cooled to 3 °C (Muscariello et al., 2005). Image analysis was performed with ImageJ 1.42 (NIH, Bethesda, MD, USA), and the following parameters were evaluated: cellular shape was determined by area measurement and maximum Feret's diameter (maximum caliper length); the solidity of cells was estimated by the ratio of the area of a cell to the area of its convex hull (Peterbauer et al., 2011). Pair-wise comparisons for statistical significance were made by Student's *t*-test.

Immunofluorescence assay for actin fiber evaluation

UMR-106 cells were cultured on coverslips for 24 h at 37 °C in a 5% CO_2 atmosphere, with serum-free DMEM in the presence of 100 μg/ml BSA or AGEs-BSA, and in the presence or absence of different doses (10^{-8} or 10^{-5} M) of alendronate. After this incubation period, the cells were fixed with 4% p-formaldehyde in PBS for 15 min, permeabilized with cold ethanol for 4 min and incubated with fluorescein-labeled phalloidin (1:100) for 1 h at room temperature. Samples were then stained with propidium iodide and coverslips were mounted in 80% glycerol-PBS. The images were taken with a Nikon Coolpix 4500 digital camera on an Eclipse E400 Nikon microscope (Tokyo, Japan), in order to determine the actin cytoskeleton structure of osteoblastic cells (Cortizo and Kreda, 2000).

Apoptosis evaluation by comet assay (single cell gel electrophoresis (SCGE) assay)

The comet assay was performed with UMR-106 osteoblasts incubated with BSA or AGEs-BSA (200 μg/ml) and/or alendronate 10^{-8} M for 24 h, following an alkaline procedure (Singh, 1996) with minor modifications. Slides were cleaned with 100% ethanol and air-dried. Two solutions containing 0.5% normal melting agarose (NMA), and 0.5% low melting agarose (LMA) solution in Ca^{2+}–Mg^{2+}-free PBS were prepared. Briefly, 150 μl of 0.5% NMA was transferred onto a pre-cleaned slide pre-coated with 1% agar (to improve adherence), spread evenly, and placed at 37 °C to solidify the agarose. Afterwards, 90 μl of 0.5% LMA together with 10.000 cells (15 μl cell suspension + 75 μl of 0.5% LMA) was applied, covered with a coverslip, and placed at 4 °C for 15 min. After this layer solidified, a third layer of 75 μl of 0.5% LMA was added, and slides placed at 4 °C for 15 min. Immediately after, slides were immersed in ice-cold freshly prepared lysis solution (2.5 M NaCl, 100 mM Na_2EDTA, 10 mM Tris, pH 10.0, 1% Triton X-100, 10% DMSO) in the dark at 4 °C overnight. Slides were then placed in a horizontal electrophoresis device filled with freshly prepared electrophoresis buffer (1 mM Na_2 EDTA, 300 mM NaOH) for 20 min at 4 °C to allow the cellular DNA to unwind, followed by electrophoresis in the same buffer at 4 °C for 20 min at 25 V and 250 mA. Slides were then neutralized with a solution of 0.4 M Tris–HCl (pH 7.5) and stained with propidium iodide. The comets were observed using a 100× objective with an Eclipse E400 Nikon microscope (Tokyo, Japan). The comet (DNA tail) size positively correlates with the level of cellular DNA breakage and alkali-labile sites. Fifty cells were counted for each condition and classified according to comet size as: grade 0 = no migration of DNA; grade 1 = short migration; grade 2 = medium migration, grade 3 = important migration with visible nucleus; grade 4 = indefinite nucleus. The results are expressed as % of each comet grade. We then calculated a parameter called total count per sample (TCS) which is derived from the following formula: TCS = (% of comet with grade 0) × 0 + (% of comet with grade 1) × 1 + (% of comet with grade 2) × 2 + (% of comet with grade 3) × 3 + (% of comet with grade 4) × 4. This parameter can range from 0 to 400 arbitrary units. Values closer to 0 represent little DNA damage, while larger values of this factor indicate significant damage to the genetic material (Collins et al., 1995).

Statistical analysis

For each experimental condition, at least three separate experiments were performed by triplicate. Data are expressed as the mean ± SEM. Statistical differences were analyzed using Student's *t*-test. Differences were considered significant when $p < 0.05$.

Results

Effect of AGEs and alendronate on cell morphology by E-SEM

Cells incubated with control BSA, were well bonded to the substratum, with a flat aspect and nuclei with prominent nucleoli (Fig. 1a). In addition, they possessed an extended cytoplasm and regular margins demonstrated by opaque structures in the E-SEM images. Osteoblasts exposed to AGEs-BSA (Fig. 1b) showed a decreased area of matrix adhesion (*i.e.* a less extended morphology) and a more voluminous shape, thus presenting high contrast regions when observed by E-SEM. Quantitative analysis of the images supports these observations: a decrease in the area of AGEs-incubated cells (Fig. 2a) and in Feret's diameter (Fig. 2b) when compared with osteoblasts incubated with control BSA.

Cells incubated with BSA and 10^{-8} M alendronate (Fig. 1c), retained the characteristics observed for BSA alone. However, cells exposed to BSA and 10^{-5} M alendronate showed fewer intercellular connections, with narrow cellular processes between neighboring cells (Fig. 1e). The solidity of cells (Fig. 2c) was also statistically decreased under this condition and was associated with an increase in the number of filopodia.

Co-incubation of cells with AGE-BSA and 10^{-8} M alendronate prevented the morphological alterations induced by AGEs-BSA, preserving a more extended morphology and a flatter shape similar to that observed for BSA alone (Fig. 1d). Image analysis quantification showed a significant increase in both cell area and Feret's diameter when compared with control BSA- and AGE-incubated cells (see Fig. 2a and b). On the contrary, co-incubation with AGEs-BSA and high doses of alendronate (10^{-5} M, Fig. 1f) potentiated the morphological changes induced by AGEs on osteoblasts: the cytoplasm was more contracted, and intercellular processes were fewer and narrower. In addition, we found that the solidity parameter decreased significantly, confirming these observations (Fig. 2c).

Effects of AGEs and alendronate on osteoblastic actin cytoskeleton

In another series of experiments, the effects of AGEs and/or alendronate on the distribution of actin fibers were investigated. Osteoblasts incubated with control BSA (Fig. 3a) showed a high density of actin stress fibers, with a longitudinal distribution (edge to edge) within the cell and multiple interconnecting processes. After incubation with AGEs-BSA (Fig. 3b), cells showed disorganized actin filaments, which were shorter and irregular and did not extend from edge to edge. Fewer processes between cells were apparent with a decrease in the area of intercellular contact.

The addition of 10^{-8} M alendronate to BSA (Fig. 3c) did not modify cell shape, although it induced an increase in the density of actin fibers *versus* osteoblasts incubated with BSA alone. However, co-incubation of cells with BSA and 10^{-5} M alendronate (Fig. 3e) induced major changes: actin fibers were considerably shorter, thicker and disorganized showing a zig-zag pattern; cells lost contact with each other or interacted through very thin intercellular processes.

Cells co-incubated with AGEs and 10^{-8} M alendronate (Fig. 3d) showed an increase in the density of actin fibers *versus* osteoblasts incubated with AGEs alone, as well as a conservation of cell shape. However, co-incubation of AGEs with 10^{-5} M alendronate (Fig. 3f) caused a major disruption of the actin cytoskeleton with very short and random fibers. This noticeably affected the shape and interconnectivity of cells, which exhibited irregular edges and only a few very thin intercellular processes (this is coincident with what has been noted for Fig. 1f). In addition the presence of a special structure near the nucleus called the geodesic dome, was observed under this condition (Fig. 3h). This structure was also seen in cells incubated with BSA and 10^{-5} M alendronate (Fig. 3g) as well as in cells exposed only to AGEs (Fig. 3b).

Effect of AGEs-modified type I collagen and alendronate on osteoblast proliferation

We next analyzed the effect of AGEs-modified collagen, the major bone matrix protein, on the viability of osteoblasts (Fig. 4). AGEs-collagen as a substratum for cell growth induced a decrease in osteoblast proliferation (89% of non-glycated collagen). Low doses of alendronate (10^{-8} M) did not affect the growth of cells plated on unmodified collagen, whereas 10^{-5} M alendronate significantly inhibited cell proliferation (30% of control collagen). On the other hand, incubation with 10^{-8} M alendronate was able to completely

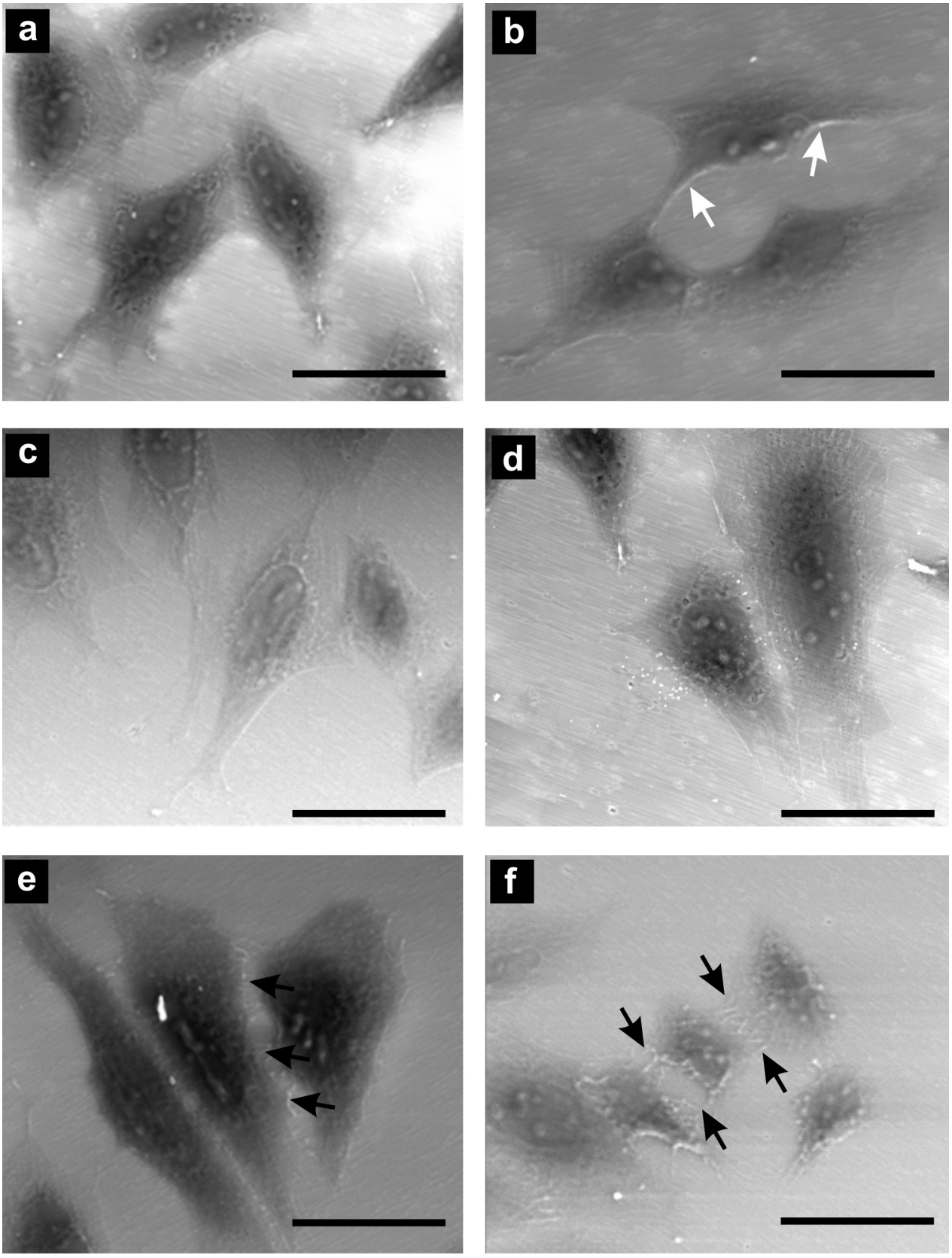

Fig. 1. E-SEM images: AGEs alter osteoblastic morphology, and this is prevented by low doses (but potentiated by high doses) of alendronate. UMR-106 cells were incubated for 24 h in the presence of either 100 μg/ml BSA (a, c, and e) or AGEs-BSA (b, d, and f), and coincubated with either 10^{-8} M alendronate (c and d) or 10^{-5} M alendronate (e and f). Scale bars = 40 μm. White arrows = high contrast regions; black arrows = cellular processes.

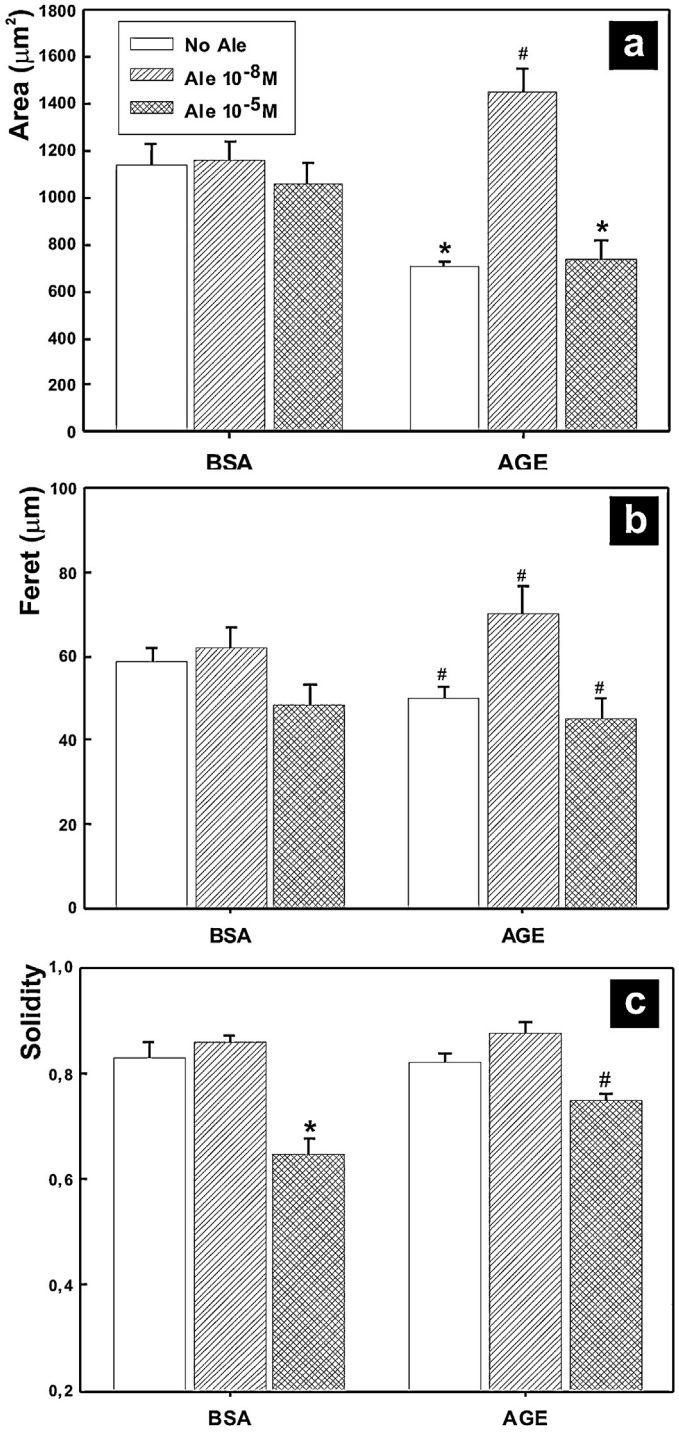

Fig. 2. Quantification of morphological parameters by image analysis of osteoblastic cells observed by E-SEM after the incubations indicated in Fig. 1. (a) Cellular area, (b) Feret's diameter and (c) solidity: ratio of cell area to convex hull area (*$p < 0.005$, #$p < 0.025$).

prevent the AGEs-collagen induced decrease in cell proliferation, whereas 10^{-5} M alendronate induced a 30% inhibition in the proliferation of these cells.

Effect of AGEs and alendronate on osteoblast apoptosis: evaluation by comet assay

Osteoblasts were incubated for 24 h with BSA or AGEs-BSA (200 μg/ml) and/or 10^{-8} M alendronate, after which apoptosis was evaluated by the comet assay as described in materials and methods section. Fifty cells were counted for each condition and graded according to DNA tail characteristics. Representative images are shown for different conditions, and results are indicated as the percentage of each comet grade (Fig. 5).

Osteoblasts incubated with BSA showed a pattern dominated by grade 0 and grade 1 comets, indicating that their nuclei are well preserved with only a small proportion of cells (6%) presenting electrophoretic migration of DNA (Fig. 5: TCS = 35.4 ± 2.5). The same pattern was observed when the cells were incubated in presence of BSA and 10^{-8} M alendronate (TCS = 49.4 ± 2.9). On the other hand, cells exposed to AGEs-BSA presented mostly grades 2, 3 and 4 comets, suggesting an increase in the apoptotic degradation of DNA induced by AGEs (TCS = 262.0 ± 6.9). Finally, cells co-incubated with AGEs-BSA and 10^{-8} M alendronate showed an intermediate situation, with a predominance of grade 1 comets (54%), followed by grade 0 (28%) and grade 2 (18%) (TCS = 91.4 ± 4.7) Thus, low doses of alendronate were able to partially prevent the AGEs-induced increase in apoptosis observed in osteoblastic cells.

Discussion

In this study, we have obtained new data using novel methods that enrich and complete our previous observations regarding the effects of AGEs on osteoblast cell morphology and adhesion to a collagenous substrate (McCarthy et al., 2004 and unpublished results). We previously showed that the accumulation of AGEs on a type I collagen matrix inhibits integrin-mediated osteoblast adhesion and spreading. Our present observations provide evidence for an AGEs-induced disruption of osteoblastic actin cytoskeleton with formation of geodesic domes, leading to significant alterations in cell morphology. In anchorage-dependent cells there are two distinctive forms of cytoskeletal arrangements: the more common actin stress fiber formation and the "geodesic dome", "geodome" or "polygonal net" formation. The latter represents a highly organized microarchitecture within the cell, consisting of ordered polygonal (triangular) elements, which typically show up in F-actin staining. The two cytoskeletal forms are believed to differ in their interaction with the ECM and their association with the underlying focal adhesions. The geodesic domes are considered as the cytoskeleton of retracted cells with reduced adhesion to the substrate, hence assuming a more spherical shape to minimize elastic energy as seen in a typical pre-stressed structure (Entcheva and Bien, 2009).

Cell adhesion to the ECM regulates cell homeostasis in multiple ways: it can take place directly or indirectly, *via* integrin-linking to the actin cytoskeleton and to growth factor receptors, thus activating or deactivating intracellular signal transduction cascades. The interruption of this connection to the ECM has detrimental effects on cell survival, leading to a specific type of apoptosis called anoikis in most non-transformed cell types (Reddig and Juliano, 2005).

Dobler et al. (2006) recently reported that the chronic vascular disease of diabetes is associated with a disruption of endothelial cell adhesion to its ECM, endangering cell survival and vascular structure. The authors show that methylglyoxal, a precursor of AGEs whose formation is increased in hyperglycemia, causes a strong change in the binding sites of integrins to type IV collagen of the vascular basement membrane, causing endothelial cell detachment, anoikis, and inhibition of angiogenesis. A previous study by other authors (Howard et al., 1996) has suggested that the cross-linking of collagen fibrils induced by their non-enzymatic glycation (which would alter the physical properties of the ECM), can lead to intracellular changes in the organization of the actin cytoskeleton. Stress fibers are involved in integrin-mediated cellular anchoring to the ECM by formation of focal adhesions, and this process can influence cell differentiation and/or survival. If the normal pattern of

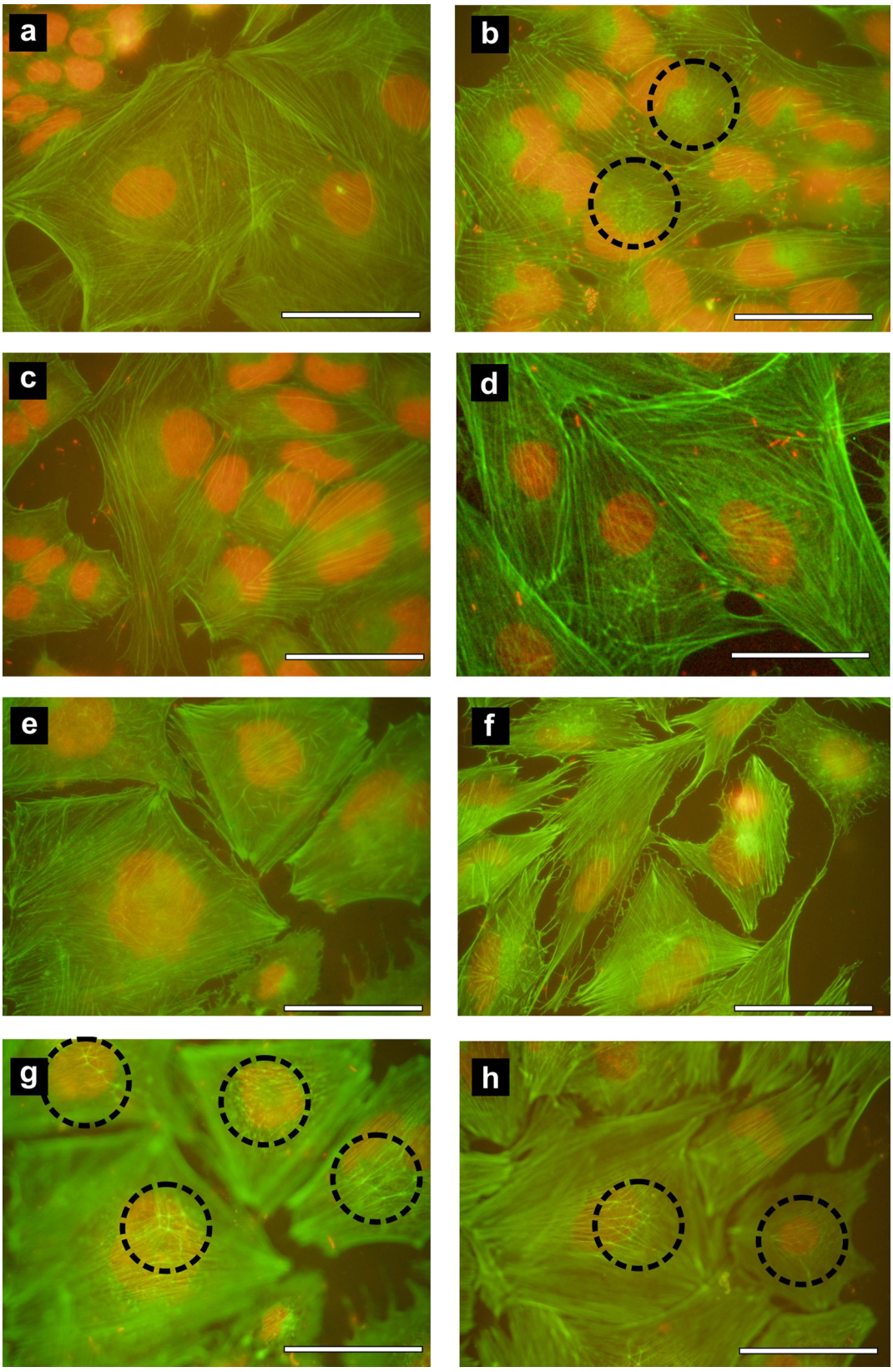

Fig. 3. Osteoblast actin cytoskeleton is disrupted by AGEs, and this is prevented by low doses (but potentiated by high doses) of alendronate. UMR-106 cells were incubated for 24 h in the presence of either 100 μg/ml BSA (a, c, e, and g) or AGEs-BSA (b, d, f, and h), and coincubated with either 10^{-8} M alendronate (c and d) or 10^{-5} M alendronate (e, f, g, and h). The cells were then incubated with FITC-phalloidine to evaluate actin fibers by direct immunofluorescence (green). Cell nuclei were stained with propidium iodide (red). Note: dotted circles indicate the presence of cellular geodesic domes. Scale bars = 50 μm. (For interpretation of the references to color in this figure legend, the reader is referred to the web version of this article.)

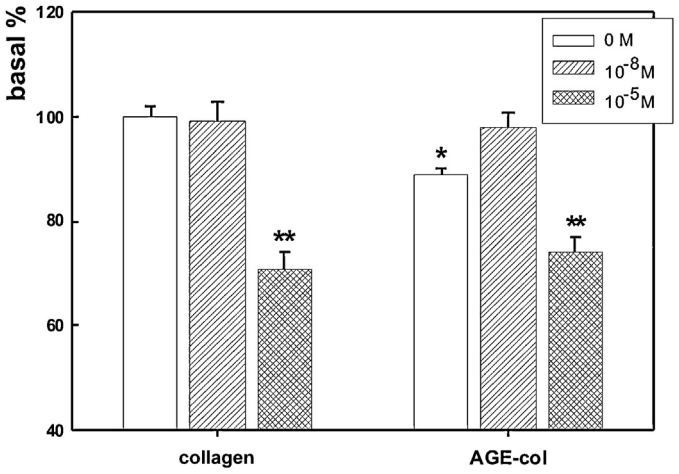

Fig. 4. Osteoblast proliferation on a type-1 collagen matrix is inhibited by AGEs modification of collagen, and this effect is prevented by low doses (but potentiated by high doses) of alendronate. UMR-106 cells were plated on collagen or AGE-collagen coated wells, and coincubated with either 10^{-8} M or 10^{-5} M alendronate for 24 h. Cell proliferation was determined by the crystal violet method ($^{*}p < 0.05$ and $^{**}p < 0.01$).

actin cytoskeleton is disrupted, osteoblasts can lose their capacity to adhere to the ECM and survive, thus shortening their life-span and functionality.

The cytoskeleton, as well as being critical for cell morphology and homeostasis, is also involved in other cellular processes such as mobility, intracellular transport and differentiation. Certain small GTP-binding proteins (G proteins) of the Ras family, such as RhoA, can influence various elements of the cytoskeleton. In particular, RhoA stabilizes the actin cytoskeleton and promotes the formation of focal adhesions in osteoblastic cells. Nitrogen-containing bisphosphonates (N-BP) such as alendronate have been shown to act by inhibiting the mevalonate pathway, thereby preventing prenylation of small GTPase signaling proteins such as RhoA. This mechanism of action has been demonstrated to be operative in osteoclasts (Bergstrom, 2000) and in osteoblasts (Idris et al., 2008).

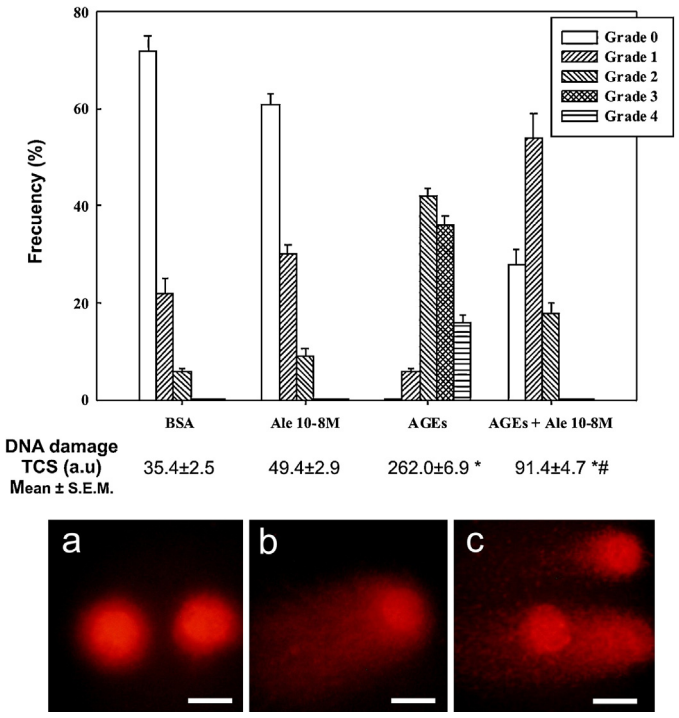

Fig. 5. Soluble AGEs induce osteoblastic apoptosis, and this effect is partially prevented by low doses of alendronate. Osteoblasts were incubated with either 200 μg/ml BSA or AGEs-BSA and/or 10^{-8} M alendronate for 24 h. The comets were sorted visually into classes 0–4 representing increasing amounts of DNA damage. The graph shows the percentage of each comet grade for different experimental conditions. The box below shows DNA damage expressed as TCS in arbitrary units (mean ± SEM) ($^{*}p < 0.005$ *versus* BSA condition, $^{\#}p < 0.005$ *versus* AGE-BSA condition). Representative images are shown for each experimental condition: (a) BSA, (b) AGE-BSA, (c) AGE-BSA and 10^{-8} M alendronate. Scale bars = 20 μm.

In the present study we have found that 10^{-8} M of alendronate, when co-incubated with BSA or AGEs-BSA, increases the density of osteoblastic actin fibers, although it does not modify either the length or distribution of the fibers nor overall cell morphology. Additionally 10^{-8} M alendronate prevents AGEs-induced alterations in osteoblastic morphology. However, when osteoblasts are exposed to higher concentrations of alendronate (10^{-5} M) striking alterations in cell morphology and in the density and distribution of actin fibers (geodesic domes) can be observed. When these high doses of alendronate are co-incubated with AGEs-BSA, the morphological and cytoskeletal disruption of osteoblasts are significantly greater than that of each agent on its own, suggesting the involvement of independent and/or additive mechanisms. For instance, AGEs could possibly be interfering with the integrin-mediated recognition of (and attachment to) the ECM, and possibly could also induce activation of RAGE (receptor for AGEs) in a mechanism involving RhoA that generates intercellular gaps, prominent stress fibers and cell contraction, as described by other authors for endothelial cells (Hirose et al., 2010). On the other hand, high-dose alendronate can affect the actin cytoskeleton and formation of focal adhesions through its actions on the geranylgeranylation of RhoA and, potentially, through these effects could influence the remodeling of bone (Kazmers et al., 2009).

The process of bone formation is multifactorial and can be regulated by multiple endogenous and/or exogenous agents that affect the survival and specific actions of osteoprogenitor cells, osteoblasts and osteocytes. For example, N-containing bisphosphonates (N-BP) such as alendronate decrease the prenylation of small GTPase signaling proteins in osteoblasts, thus altering their functionality (Idris et al., 2008). These authors have found that N-BP induce apoptosis of osteoblasts at concentrations of 10^{-4} M. In addition, our group has previously shown a biphasic effect of bisphosphonates on osteoblastic growth and differentiation, with an increase in both parameters at low concentrations of bisphosphonates, and a decrease at 10^{-4}–10^{-5} M (Vaisman et al., 2004). Plotkin et al. (2006) have demonstrated that N-BP can prevent osteoblast and osteocyte apoptosis *in vivo* and *in vitro*, and have proposed that the anti-fracture actions of these exogenous agents could result in part from a preservation of the integrity of the osteocyte network. Further studies are clearly needed to fully define the mode of action of N-BP on bone-forming cells.

AGEs are endogenous agents that accumulate in the bone ECM of patients with diabetes. It has previously been shown that AGEs can decrease bone forming potential, by inhibiting osteoblastic attachment to the ECM, proliferation, differentiation and mineralization (McCarthy et al., 1997, 2001, 2004), and by increasing apoptosis in this cell type (Gangoiti et al., 2008). Accumulation of AGEs induces oxidative stress, and *in vitro* studies have found that oxidative stress induces damage and apoptosis in osteoblasts and inhibits their differentiation (Hamada et al., 2009). AGEs-modified collagen induces apoptosis in primary cultures of osteoblasts or MC3T3-E1 cells *in vitro*, and this effect is mediated by AGEs-RAGE interaction (Alikhani et al., 2007). However, all the harmful actions of AGEs on osteoblasts (including induction of apoptosis) can be completely prevented by low concentrations of N-BP (Gangoiti et al., 2008). In the present study we have been able to reproduce our previous observations regarding the anti-apoptotic effect of low doses

of alendronate in osteoblasts exposed to AGEs (albeit using a different method to evaluate apoptosis: the comet assay instead of the Annexin V-propidium iodide assay). This anti-apoptotic effect could provide an explanation for the prevention, by low doses of N-BP, of the anti-proliferative effect of AGEs observed in osteoblasts (Gangoiti et al., 2008).

In conclusion, our present results provide evidence for an AGEs-induced disruption of the osteoblastic actin cytoskeleton with the formation of geodesic domes, as well as significant alterations in cell morphology with a decrease in microscopically visible cell-cell and cell-substratum interaction, leading to an increase in osteoblast apoptosis and a decrease in osteoblast proliferation. High concentrations of alendronate (such as could be expected in an osteoclastic lacuna) further increase osteoblastic morphological and cytoskeletal alterations. On the other hand, low doses of alendronate (compatible with extracellular fluid levels to which an osteoblast could be exposed for most of its life cycle) (Spreafico et al., 2006) do not affect cell morphology on their own, but are able to prevent the AGEs-induced alterations in osteoblastic morphology, apoptosis and proliferation.

Acknowledgments

We wish to thank Dr. Ostrowsky, Laboratorios Elea, Argentina for the donation of alendronate. This study was partially supported by grants from the Universidad Nacional de La Plata, Agencia Nacional de Promoción Científica y Tecnológica (PIC 1083 BID-1728/O.C.-A.R) and Comisión de Investigaciones Científicas de la provincia de Buenos Aires (CICPBA). M.V.G. is a postdoctoral fellow of C.O.N.I.C.E.T., A.M.C. is a member of the Carrera del Investigador, C.I.C.P.B.A., and A.D.M. is a part-time researcher and Professor, U.N.L.P.

References

Alikhani M, Alikhani Z, Boyd C, MacLellan CM, Raptis M, Liu R, et al. Advanced glycation end products stimulate osteoblast apoptosis via the MAP kinase and cytosolic apoptotic pathways. Bone 2007;40:345–53.

Barbosa J, Oliveira S, Tojal e Seara L. O papel dos produtos finais da glicação avançada (AGEs) no desencadeamento das complicações vasculares do diabetes. Arq Bras Endocrinol Metabol 2008;52:940–50.

Bergstrom JD. Alendronate is a specific, nanomolar inhibitor of farnesyl diphosphate synthase. Arch Biochem Biophys 2000;373:231–41.

Brownlee M. The pathobiology of diabetic complications: a unifying mechanism. Diabetes 2005;54:1615–25.

Collins AR, Ma AG, Duthie SJ. The kinetics of repair of oxidative DNA damage (strand breaks and oxidised pyrimidines) in human cells. Mutat Res 1995;336:69–77.

Cortizo AM, Kreda S. Vanadium induced alterations in cytoeskeleton and protein tyrosine-phosphorilation in osteoblast cell lines. In: Centeno JA, Collery PH, Vernet G, Finkelman RB, Gibb H, Etienne JC, editors. Metal ions in biology and medicine, vol. 6. Paris: John Libbey Eurotext; 2000. p. 714–6.

Dagdelen S, Sener D, Bayraktar M. Influence of type 2 diabetes mellitus on bone mineral density response to bisphosphonates in late postmenopausal osteoporosis. Adv Ther 2007;24:1314–20.

Dobler D, Ahmed N, Song L, Eboigbodin KE, Thornalley PJ. Increased dicarbonyl metabolism in endothelial cells in hyperglycemia induces anoikis and impairs angiogenesis by RGD and GFOGER motif modification. Diabetes 2006;55:1961–9.

Entcheva E, Bien H. Mechanical and spatial determinants of cytoskeletal geodesic dome formation in cardiac fibroblasts. Integr Biol 2009;1:212–9.

Gangoiti MV, Cortizo AM, Arnol V, Felice JI, McCarthy AD. Opposing effects of bisphosphonates and advanced glycation end-products on osteoblastic cells. Eur J Pharmacol 2008;600:140–7.

Hamada Y, Fujii H, Fukagawa M. Role of oxidative stress in diabetic bone disorder. Bone 2009;45:S35–8.

Hein G, Wiegand R, Lehmann G, Stein G, Franke S. Advanced glycation end-products pentosidine and N^{ϵ}-carboxymethyllysine are elevated in serum of patients with osteoporosis. Rheumatology 2003;42:1242–6.

Hirose A, Tanikawa T, Mori H, Okada Y, Tanaka Y. Advanced glycation end products increase endothelial permeability through the RAGE/Rho signaling pathway. FEBS Lett 2010;584:61–6.

Howard E, Ahern-Moore R, Tomasek J. Cellular contraction of collagen lattices is inhibited by nonenzymatic glycation. Exp Cell Res 1996;228:132–7.

Idris AI, Rojas J, Greig IR, Van't Hof RJ, Ralston SH. Aminobisphosphonates cause osteoblast apoptosis and inhibit bone nodule formation *in vitro*. Calcif Tissue Int 2008;82:191–201.

Kazmers N, Ma SA, Yoshida T, Stern P. Rho GTPase signaling and PTH 3-34, but not PTH 1-34, maintain the actin cytoskeleton and antagonize bisphosphonate effects in mouse osteoblastic MC3T3-E1 cells. Bone 2009;45:52–60.

McCarthy AD, Etcheverry SB, Bruzzone L, Cortizo AM. Effects of advanced glycation end-products on the proliferation and differentiation of osteoblast like cells. Mol Cell Biochem 1997;170:43–51.

McCarthy AD, Etcheverry SB, Bruzzone L, Lettieri G, Barrio DA, Cortizo AM. Non-enzymatic glycosylation of a type I collagen matrix: effects on osteoblastic development and oxidative stress. BMC Cell Biol 2001;2:16.

McCarthy AD, Uemura T, Etcheverry SB, Cortizo AM. Advanced glycation endproducts interfere with integrin-mediated osteoblastic attachment to a type-I collagen matrix. Int J Biochem Cell Biol 2004;36:840–8.

Muscariello L, Rosso F, Marino G, Giordano A, Barbarisi M, Cafiero G, et al. A critical overview of ESEM applications in the biological field. J Cell Physiol 2005;205:328–34.

Okajima T, Nakamura K, Zhang H, Ling N, Tanabe T, Yasuda T. Sensitive colorimetric bioassays for insulin-like growth factor (IGF) stimulation of cell proliferation and glucose consumption: use in studies of IGF analogs. Endocrinology 1992;130:2201–12.

Osma JF, Toca-Herrera JL, Rodríguez-Couto S. Environmental, scanning electron and optical microscope image analysis software for determining volume and occupied area of solid-state fermentation fungal cultures. Biotechnol J 2011;6:45–55, Erratum in: Biotechnol J 2011; May 6:609.

Partridge NC, Alcorn D, Michelangeli VP, Ryan G, Martin TJ. Morphological and biochemical characterization of four clonal osteogenic sarcoma cell lines of rat origin. Cancer Res 1983;43:4308–15.

Peterbauer T, Yakunin S, Siegel J, Hering S, Fahrner M, Romanin C, et al. Dynamics of spreading and alignment of cells cultured in vitro on a grooved polymer surface. Journal of Nanomaterials Special issue on pharmaceutical applications of polymeric nanomaterials 2011., http://dx.doi.org/10.1155/2011/413079, Article N 2.

Plotkin LI, Manolagas SC, Bellido T. Dissociation of the pro-apoptotic effects of bisphosphonates on osteoclasts from their anti-apoptotic effects on osteoblasts/osteocytes with novel analogs. Bone 2006;39:443–52.

Reddig PJ, Juliano RL. Clinging to life: cell to matrix adhesion and cell survival. Cancer Metastasis Rev 2005;24:425–39.

Schwartz AV. Diabetes mellitus: does it affect bone? Calcif Tissue Int 2003;73:515–9.

Sharp PS, Rainbow S, Mukhergee S. Serum levels of low molecular weight advanced glycation end products in diabetic subjects. Diabet Med 2003;20:575–9.

Singh NP. Microgel electrophoresis of DNA from individual cells: principles and methodology. In: Pfeifer GP, editor. Technologies for detection of DNA damage and mutations. New York: Plenum Press; 1996. p. 3–24.

Small JV, Kaverina I, Krylyshkina O, Rottner K. Cytoskeleton cross-talk during cell motility. FEBS Lett 1999;452: 96–9.

Spreafico A, Frediani B, Capperucci C, Gambera D, Ferrata P, Baldi F. Anabolic effects and inhibition of interleukin 6 production induced by neridronate on human osteoblasts. Reumatismo 2006;58:288–300.

Stabentheiner E, Zankel A, Pölt P. Environmental scanning electron microscopy (ESEM) – a versatile tool in studying plants. Protoplasma 2010;246:89–99.

Uroukov IS, Patton D. Optimizing environmental scanning electron microscopy of spheroidal reaggregated neuronal cultures. Microsc Res Tech 2008;71:792–801.

Vaisman DN, McCarthy AD, Cortizo AM. Bisphosphonates affect the growth, differentiation and cytoskeleton of UMR106 osteoblasts in culture. Osteoporos Int 2004;15(Suppl. 1):S133.

Viereck V, Emons G, Lauck V, Frosch KH, Blaschke S, Grundker C. Bisphosphonates pamidronate and zoledronic acid stimulate osteoprotegerin production by primary human osteoblasts. Biochem Biophys Res Commun 2002;291:680–6.

Yamauchi M, World Health Organization. Absolute risk for fracture and WHO guideline. Treatment of patients with secondary osteoporosis. Clin Calcium 2007;17:1106–13.